Dynamics of injected electron cooling in GaAs

J. R. Hayes
Bell Communications Research, Murray Hill, New Jersey 07974

A. F. J. Levi and W. Weigmann
AT&T Bell Laboratories, Murray Hill, New Jersey 07974

(Received 10 February 1986; accepted for publication 25 March 1986)

Using the technique of hot-electron spectroscopy we have measured the change in hot-electron spectra with transit region width enabling us to obtain a dynamic picture of injected hot-electron cooling in n^+ GaAs. All features in the spectra have been identified and "ballistic" transport has been observed for samples having narrow transit region widths (<850 Å) while near diffusive transport has been observed for samples having wide transit region widths (>1700 Å). With increasing transit region width, rather than the electron distribution shifting *en masse* to lower energies, electrons are removed from the initial injected peak and scattered to lower energies close to the Fermi energy. This process of electron cooling is dramatically illustrated by measuring the magnetic field dependence of the hot-electron spectra.

The advent of thin-film epitaxial crystal growth techniques makes possible the fabrication of many semiconductor structures which incorporate abrupt potential steps in the conduction and valence bands, e.g., unipolar transistors,[1] heterojunction bipolar transistors,[2] and heterojunction lasers.[3] Charge carriers injected over such potential steps obtain extreme nonequilibrium distributions which, to varying degrees, affect device performance. In order to better understand the operation of such devices we invented "hot-electron spectroscopy," a technique which enabled us to probe directly the dynamics of injected, nonequilibrium electrons in semiconductors.[4] Using this technique we were the first to observe "ballistic" transport in a semiconductor[5]; a result later confirmed by Heiblum *et al.*[6] In addition to this observation, which is important in itself, understanding the cooling of an injected charge distribution is necessary for a complete understanding of today's electronic devices and future modeling. The results discussed here were obtained using single crystal GaAs samples grown by molecular beam epitaxy at 650 °C. The energy-band structure of the grown sample is shown schematically in Fig. 1 and consists of three n^+ (Si impurity concentration 1×10^{18} cm^{-3}) GaAs regions separated by two bulk triangular potential barriers. The first n^+ region (forming the n^+ buffer layer) was typically 8000 Å thick and was followed by the growth of a nominally undoped layer in which a thin (~100 Å) Be impurity layer was incorporated to form the "hot-electron analyzer" triangular potential barrier in the conduction band. The transit region was then grown, which for the four samples to be discussed here had widths of 650, 850, 1200, and 1700 Å. Following the growth of the transit region a second triangular barrier was formed similar to the first, but having a narrower Be charge sheet so that the hot-electron injector barrier energy was slightly lower than that of the analyzer. The epilayer growth was completed by the addition of a thin (~2000 Å) n^+ cap layer. The sample was chemically etched into two level mesa structures in order that the three n^+ regions could be contacted individually. Ohmic contacts were made to these regions by rapidly thermally annealing an evaporated Au–Sn alloy.

Since the structure shown in Fig. 1 resembles an unipolar transistor we use standard transistor notation to describe the currents and voltages involved. In operation the hot-electron injector at the emitter/base junction is biased negative with respect to the grounded transit region such that a well-collimated and almost monoenergetic nonequilibrium electron distribution is injected into the transit region. While in the transit region, the injected hot electrons may scatter inelastically with the electron/phonon system or elastically with ionized impurities (in degenerate n-type GaAs, with a carrier concentration $\sim10^{18}$ cm^{-3}, the main scattering mechanism for hot electrons is inelastic collision with coupled plasmon/phonon modes). At the far end of the transit region the resulting electron distribution is measured by using the base/collector triangular potential barrier as a hot-electron analyzer. By measuring dI_c/dV_{bc} as a function of V_{bc} we have a means of obtaining spectroscopic information on the hot-electron momentum distribution at the far end of the transit region.

In intrinsic or very lightly doped GaAs, hot electrons with energies greater than the longitudinal optical (LO) phonon energy are inelastically scattered by the emission of LO phonons. However, at carrier concentrations of $\sim1\times10^{18}$ cm^{-3} the long wavelength collective oscillatory (plasmon) mode of the n^+ electron gas is close in energy to that of the LO phonons. These two longitudinal oscillations do not exist independently of each other but interact strongly to create a coupled plasmon/phonon system. It is therefore physically incorrect to describe hot-electron scattering in terms of separate contributions from phonon and plasmon modes in n^+ GaAs. In addition to hot electrons being inelastically scattered from long wavelength coupled plasmon/phonon collective modes they may also scatter via the creation of single electron-hole pairs (the so called electron-hole continuum). With decreasing wavelength the collective modes are damped by the continuum leaving only the continuum and optical phonons contributing to the scattering.

In this letter we do not attempt to document details of the calculation of inelastic scattering rates, as this has been done elsewhere,[5,7] rather we use the results to discuss the evolution of the hot-electron spectra. The calculated inelastic scattering rate for hot electrons as a function of electron energy in n^+ GaAs doped to 1×10^{18} cm^{-3} is shown in Fig. 2 together with that for intrinsic material. Hot-electron ener-

 0003-6951/86/201365-03$01.00

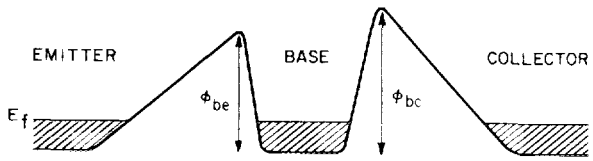

FIG. 1. Schematic of the conduction-band minimum of a hot-electron spectrometer fabricated in a single crystal of GaAs. The long and short arms of the triangular barriers have an aspect ratio of 10 with a short arm width of 150 Å.

gies greater than 300 meV above the conduction-band minimum are not considered in the calculation since for energies greater than this, other details, such as intervalley scattering, must be included. Our calculations of hot-electron inelastic scattering rates play an important role aiding understanding of hot-electron spectra.

Figure 3 shows spectra of samples measured at 4.2 K having the same n-type doping level of 1×10^{18} cm^{-3} and similar injection energies but different transit regions widths of (a) 650, (b) 850, (c) 1200, and (d) 1700 Å. The sequence of diagrams shows the evolution of the hot-electron distribution with distance from the step potential that injected a collimated beam of almost monoenergetic hot electrons into the transit region. Sample 3(a), having the narrowest transit region width, shows two distinct features; a peak at high barrier energies (low voltage bias V_{bc}) which we attribute to "ballistic" electrons, i.e., that part of the initial distribution which has not been scattered, and a second narrower peak at lower analyzer barrier energies (high V_{bc}), close to the Fermi energy, attributed to electrons excited from the Fermi sea, i.e., the electron distribution in the transit region has been "heated" by interaction with the injected electrons. Now consider Fig. 3(b) which shows results obtained from a sample having a transit region width of 850 Å. In this case the "ballistic" peak can only just be seen and most electrons have been scattered and are collected at lower barrier potentials (greater base/collector voltage). Such a characteristic may be understood by considering the energy-dependent

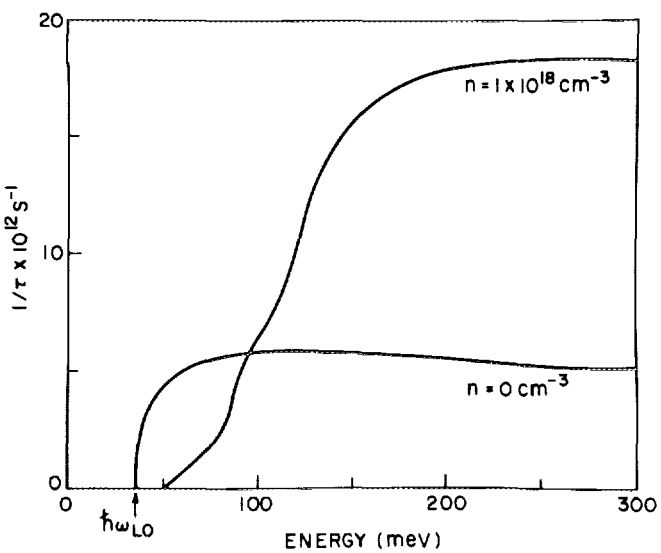

FIG. 2. Calculated total inelastic electron scattering rate as a function of injected electron energy measured from the conduction-band minimum for n^+ GaAs doped to $n = 10^{18}$ cm^{-3}. The scattering rate for intrinsic ($n = 0$ cm^{-3}) material is also shown.

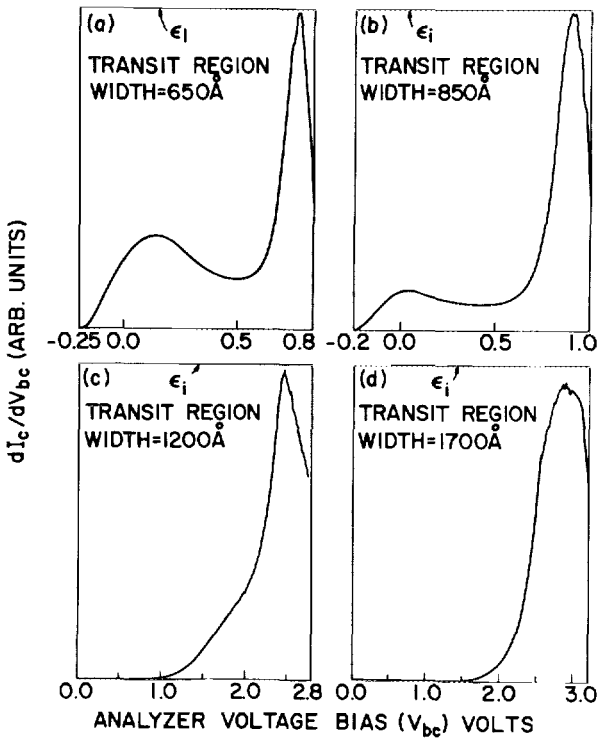

FIG. 3. Measured hot-electron spectra for four samples differing only in base width; (a) 650, (b) 850, (c) 1200, and (d) 1700 Å. The injection energy ϵ_i is indicated for each spectrum.

scattering rate detailed in Fig. 2 since the electrons are injected with energy, ~250 meV, their scattering rate is very high. However, once they have lost energy such that they are only 150 meV or less above the conduction-band minimum their scattering rate decreases and electrons begin to accumulate at lower energies. Figure 3(c) shows the progression of this process by increasing the transit region width to 1200 Å. There is little evidence of the initial injected peak and a large low-energy peak which includes many electrons scattered from high energies as well as those excited from the Fermi sea. Finally Fig. 3(d) shows a spectrum obtained from a sample with a 1700-Å-thick transit region width in which only the low-energy peak remains, containing contributions from both the injected electrons and those excited from the Fermi sea. In order to highlight the effect of increased transit region width we have applied a magnetic field to the sample having the narrowest transit region width.

When a magnetic field is applied perpendicular to the direction of electron injection a circular orbit is imposed on the trajectory of the injected electrons. This increases the length hot electrons must travel to traverse the base, giving them a greater probability of scattering, also the electrons' component of normal momentum at the analyzer is reduced so that they are collected at lower barrier energies. Hence, by applying a magnetic field we have a way of independently adjusting the hot-electron interaction length within the device.[8] In Fig. 4(a) we show the variation of the hot-electron spectrum measured using the sample with a 650 Å transit region width for the indicated values of magnetic field.

As may be seen in Fig. 4(a) with increasing magnetic field the high energy, "ballistic" peak at V_{bc} ~0.1 V bias shifts to larger V_{bc} (lower collector barrier energy) resulting

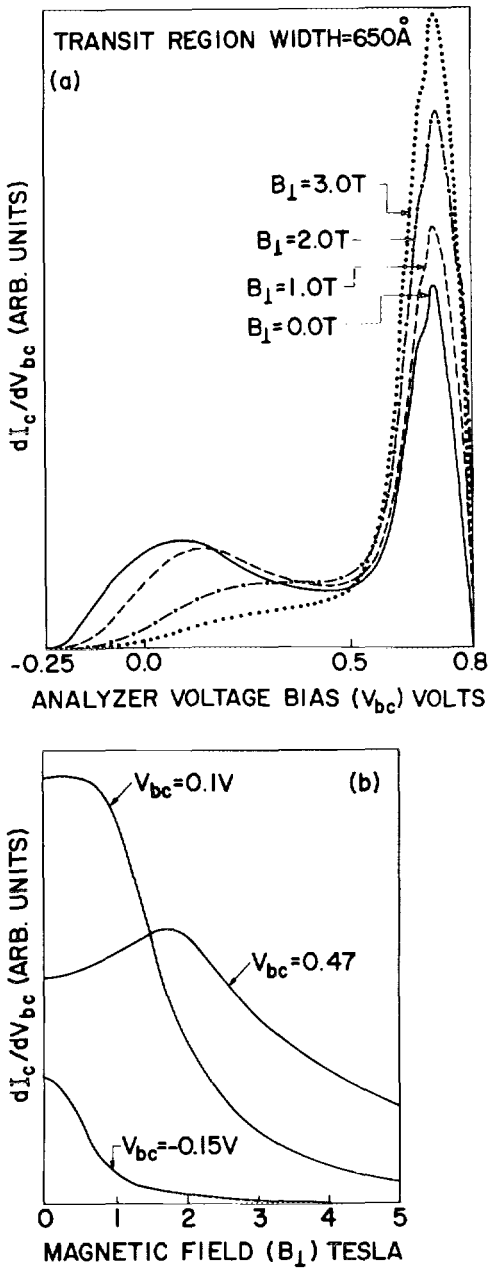

FIG. 4. (a) Variation in the hot-electron spectrum shown in Fig. 3(a) for the indicated values of magnetic field applied perpendicular to the direction of current injection. (b) Magnetic field dependence of the hot-electron spectrum in (a) for the indicated fixed values of V_{bc}.

from the change in the component of normal momentum of electrons arriving at the analyzer. We also note that the intensity of the "ballistic" peak decreases and spectral weight is transferred to lower collector barrier energies indicating that the electrons transiting the base have suffered collisions due to the increased effective transit distance in a magnetic field. The peak at low collector barrier energies ($V_{bc} \sim 0.7$ V) broadens and increases in intensity with increasing magnetic field. Qualitatively this is expected since both more electrons are excited from the Fermi sea and an increased number of hot electrons are inelastically scattered down to low energies. For clarity in Fig. 4(b) we plot the magnetic field dependence of the hot-electron spectrum for the indicated values of V_{bc}. The application of a magnetic field parallel to the direction of injected current has no effect on the measured hot-electron spectra. This is expected since, in this case, injected electrons follow a helical path between collisions so that the effective path length between emitter and collector is unchanged.

In conclusion, we have measured the evolution of hot-electron spectra with increasing base width, showing the transition from "ballistic" electron transport (small transit region width) to near diffusive transport (large transit region width). It was shown that the initial injected distribution does not shift *en masse* to lower energies but that electrons are extracted from it by strong inelastic scattering. Those inelastically scattered electrons then mix in with electrons excited from the Fermi sea causing a significant increase in the low-energy peak. Such information is important for a complete understanding of today's electronic devices and will be essential for the design of future electron injection devices.

[1] J. M. Shannon, IEE J. Solid State Electron Devices **3**, 142 (1979).
[2] V. I. Ryzhil, V. A. Fedirko, and I. I. Khmyrova, Sov. Phys. Semicond. **18**, 257 (1984).
[3] H. C. Casey and M. B. Panish, *Heterostructure Lasers*, Part A and B (Academic, London, 1978).
[4] J. R. Hayes, A. F. J. Levi, and W. Weigmann, Electron. Lett. **20**, 851 (1984); J. R. Hayes, A. F. J. Levi, and W. Weigmann, Phys. Rev. Lett. **54**, 1570 (1985).
[5] J. R. Hayes, A. F. J. Levi, A. C. Gossard, and W. Weigmann, invited talk given at the Meeting of the American Physical Society, Baltimore, March 1985, and A. F. J. Levi, J. R. Hayes, P. M. Platzman, and W. Weigmann, Phys. Rev. Lett. **55**, 2071 (1985).
[6] M. Heiblum, M. I. Nathan, D. C. Thomas, and C. M. Knoedler, Phys. Rev. Lett. **55**, 2200 (1985).
[7] A. F. J. Levi, J. R. Hayes, P. M. Platzman, and W. Weigmann, Physica B **134**, 480 (1985).
[8] J. R. Hayes, A. F. J. Levi, and W. Weigmann, Appl. Phys. Lett. **47**, 964 (1985).